JACS
JOURNAL OF THE AMERICAN CHEMICAL SOCIETY
Article
pubs.acs.org/JACS

# Characterizing Intermediates Along the Transition from Polyproline I to Polyproline II Using Ion Mobility Spectrometry-Mass Spectrometry

Liuqing Shi,[†] Alison E. Holliday,[‡,∥] Huilin Shi,[†] Feifei Zhu,[†] Michael A. Ewing,[†] David H. Russell,[§] and David E. Clemmer*,[†]

[†]Department of Chemistry, Indiana University, 800 Kirkwood Avenue, Bloomington, Indiana 47405, United States
[‡]Department of Chemistry and Biochemistry, Swarthmore College, Swarthmore, Pennsylvania 19081, United States
[§]Department of Chemistry, Texas A&M University, College Station, Texas 77843, United States

Supporting Information

**ABSTRACT:** Polyproline exists predominately as the all-*cis* polyproline I (PPI) helix in aliphatic alcohols, whereas the all-*trans* polyproline II (PPII) helix is favored in aqueous solutions. Previous ion mobility spectrometry-mass spectrometry (IMS-MS) work demonstrates that the gas-phase conformations of polyproline ions can be related to the corresponding PPI and PPII helices in solution [*J. Phys. Chem. B* **2004**, 108, 4885]. Here, we use IMS-MS to examine the detailed intermediate steps associated with the process of Polyproline-13 (Pro13) conversion from the PPI helix to the PPII helix upon solvent exchange. Collision cross section distributions of Pro13 $[M + 2H]^{2+}$ ions obtained at different transition times indicate the presence of two major conformers, identified as the PPI and PPII helices, and six conformers that appear as subpopulations of polyproline. Further analysis shows a transition mechanism with sequential *cis*–*trans* isomerizations followed by a parallel process to establish PPII and two smaller subpopulations at equilibrium. Temperature-dependent studies are used to obtain Arrhenius activation parameters for each step of the mechanism, and molecular dynamics simulations provide insight about the structures of the intermediates. It appears that prolines sequentially flip from *cis* to *trans* starting from the *N*-terminus. However, after the first few transitions, possible steps take place at the center of the peptide chain; subsequently, several pathways appear to be accessible at the same time. Our results reflect the existence of stable subpopulations in polyprolines and provide new insight into the structural changes during the transition process of polyproline peptides converting from PPI to PPII in aqueous solution.

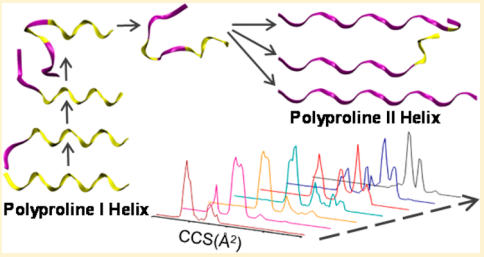


## INTRODUCTION

While most amino acids form nearly exclusively *trans* peptide bonds, proline can adopt both *cis* and *trans* conformations, a result of the lack of intramolecular hydrogen bonds and the steric constraint imposed by the side-chain pyrrolidine ring.[1,2] It has been shown that proline forms *cis* peptide bonds at a frequency (~5%) significantly higher than any other natural amino acid (<0.1%).[3] *Cis*–*trans* isomerization of proline is implicated in the conformational heterogeneity of proteins and peptides and is also involved in various biological processes, such as protein folding, cell signaling, and ion-channel gating.[4−14] Polyproline has become a valuable model system to gain a better understanding of proline isomerization. In solution and in the solid state, polyproline exists predominantly as two conformations known as polyproline I (PPI) and polyproline II (PPII).[15] Figure 1 shows the geometries of the PPI helix and the PPII helix for a 13-residue polymer. PPI is a right-handed helix with all residues in the *cis* form, whereas PPII is a more elongated left-handed helix with all residues in the *trans* form. *Cis*–*trans* isomerization of proline residues therefore leads to interconversion between these two conformations.[16−24]

Prior work has shown that that PPI, which is stabilized by van der Waals forces, is present in hydrophobic environments such as aliphatic alcohols; in contrast, PPII is favored in aqueous solutions, and its stability is attributed to the formation

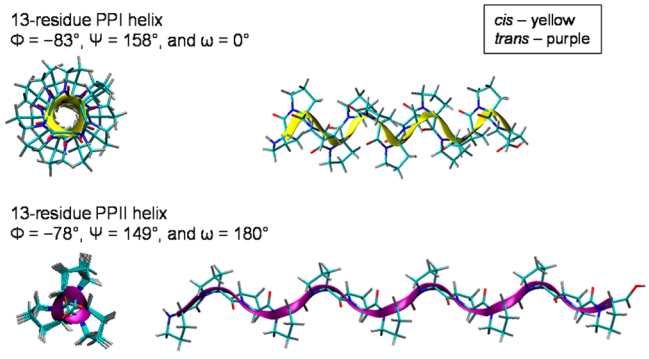


**Figure 1.** Representation of structures for Pro13. The PPI helix (Φ = −83°, Ψ = 158°, and $\omega$ = 0°) contains all *cis*-residue forms; PPII (Φ = −78°, Ψ = 149°, and $\omega$ = 180°) contains all *trans*-residue forms. Torsion angles are taken from ref 15. For each structure, two views are provided for clarity.

**Received:** June 12, 2014
**Published:** August 8, 2014

   dx.doi.org/10.1021/ja505899g | *J. Am. Chem. Soc.* 2014, 136, 12702−12711

of hydrogen bonds between water molecules and the carbonyl groups along the peptide backbone.[2,25−27] By changing the solvent composition, reversible transitions between PPI and PPII can be induced in solution. This process has been studied by various spectroscopic techniques, including optical rotation dispersion,[18−20,28] vibrational circular dichroism,[23] nuclear magnetic resonance (NMR),[29] and Raman spectroscopy.[30] Molecular dynamics[31] and ab initio free energy calculations[32] have identified sequential isomerization in a zipper-like pattern as a potential mechanism for the transition from PPI to PPII in solution. This is consistent with findings from NMR[29] and enzymatic[33] studies. However, there remains a question of whether the transition starts at the N-terminus[31,33] or the C-terminus[29,32] of the polypeptide chain. Evidence of the presence of a single intermediate in the polyproline transition has been observed using Fourier transform infrared spectroscopy and electronic/vibrational circular dichroism,[23] but detailed structural information about intermediates has not yet been measured.

Polyproline has also received considerable attention due to the high propensity of the PPII helical structure in collagens and in the disordered regions of proteins.[34−38] The PPII helix formed from polyproline was, until recently, seen as such a well-defined system that it was used as a molecular ruler to calibrate end-to-end distances in Förster resonance energy transfer (FRET) experiments.[39] However, emerging theoretical and experimental evidence indicates a complex conformer landscape for polyproline in aqueous solution. Using single molecule FRET,[40−42] photoinduced electron transfer,[43] and NMR, deviations in the PPII helix are observed in aqueous solutions; the presence of a stable heterogeneous subpopulation containing *cis* residues has been proposed based on observed end-to-end distances and computational models.[32,44−46] Enzymatic hydrolysis analysis suggests that any *cis* bonds that are present at the conclusion of the transition to PPII must be near the C-terminus.[33]

In this study, we use ion mobility spectrometry-mass spectrometry (IMS-MS) to explore the structural transitions of a 13-residue polyproline peptide (Pro13) in solution. IMS-MS has recently emerged as a powerful tool for the separation and characterization of peptides and proteins.[47−50] IMS is a rapid gas-phase separation technique; resolution of structures on the basis of collision cross section and charge typically occurs on a millisecond time scale. Investigating gas-phase conformations can contribute to the fundamental understanding of protein and peptide structures in solution.[51−57] During electrospray ionization (ESI), populations of structures that are associated with solution equilibria can be transferred to the gas phase where they can be analyzed by a range of MS techniques.[58−63] Although gas-phase structures may be dissimilar from their solution states due to the absence of solvents, several groups have shown that different solution structures can still be separated by IMS based on differences in their gas-phase collision cross sections.[54,55,64,65] Prior work has shown that the structures of gas-phase polyproline ions can be linked to the PPI and PPII conformations in solution by measuring cross section distributions.[66]

In the present study, we use IMS-MS to investigate the conformational changes of Pro13 after its solution environment is exchanged from 1-propanol to water. Two main peaks are found in the cross section distribution for Pro13 $[M + 2H]^{2+}$ ions formed in 1-propanol, and we observe two high-abundance conformers in the distribution generated from aqueous solution. Multiple gas-phase conformations are present during the transition process from PPI to PPII, providing the first experimental evidence of structurally distinct intermediates along the transition pathway. Analysis of abundance profiles for each conformation as a function of transition time gives mechanistic information about the transition, and analysis at several different solution temperatures allows us to calculate the Arrhenius activation parameters associated with each step. To correlate populations that are present in solution to the specific conformers that are observed in the gas phase, we have carried out molecular dynamic simulations for the formation of Pro13 $[M + 2H]^{2+}$ gas-phase ions and thus discuss a possible pathway for the solution-phase transition of Pro13 between the PPI and PPII helices.

## EXPERIMENTAL SECTION

**Synthesis of Pro13.** The Pro13 sample (having an isotopic molecular weight of 1279.7) was generated on a modified Applied Biosystems 430A synthesizer (Applied Biosystems, Foster City, CA) by a standard Boc solid-phase peptide synthesis protocol.[67] Reagents were purchased from Midwest Biotech (Indianapolis, IN) except where noted. In this synthesis, the C-terminal residue was anchored to phenylacetamidomethyl (PAM) resin beads. At the beginning of the synthesis, 0.2 mmol of Boc Pro-Pam resin was placed in an Applied Biosystems reaction vessel (Applied Biosystems, Foster City, CA), and the activation of amino acids (2 mmol) was performed with the addition of 0.5 M 3-(diethoxy-phosphoryloxy)-3*H*-benzo[*d*][1,2,3]-triazin-4-one (purchased from Aapptec, Louisville, KY) and *N*,*N*-diisopropylethylamine (11:1 v/v).[68] In the following coupling reactions, trifluoroacetic acid (TFA) was applied to remove the N-terminal protecting group. After the completion of the chain elongation, the deprotected peptide resin was stirred in an ice bath for 1 h in the presence of hydrogen fluoride (HF) and *p*-cresol (95:5 v/v) followed by *in vacuo* HF evacuation. Peptides were next precipitated in diethyl ether, collected by filtration, and washed with diethyl ether. Finally, the residues were extracted into dilute aqueous acetic acid and freeze-dried. The dried material was used without further purification.

**Sample Preparation.** The Pro13 sample was dissolved in 1-propanol (160 $\mu$M) and then incubated at 37 °C for 72 h to ensure that the equilibrium structures were produced. The initiation of the transition from PPI to PPII was achieved by diluting the 1-propanol solution with $H_2O$ and acetic acid (HOAc) to a final composition of 10:88:2 1-propanol/$H_2O$/HOAc (v/v/v) containing 16 $\mu$M Pro13. The transition processes were measured at five different temperatures (5, 15, 23, 35, and 45 °C), and solutions were kept in a water bath at the appropriate temperature for an equilibration period prior to dilution and for the duration of the timed experiment. Aliquots were removed by pipet at defined time intervals, placed into a sample tray held at 4 °C, and then immediately sampled for analysis. All experiments were carried out in triplicate. To represent time zero for each of the five temperatures studied, a 16 $\mu$M solution of Pro13 was also prepared in 98:2 1-propanol/HOAc (v/v), and this solution was incubated at the corresponding temperature for 72 h to ensure that the equilibrium distribution was reached.

**Instrumentation.** Detailed descriptions of IMS-MS theory[69−73] and instrumentation[48,74−76] have been reported elsewhere; a brief summary is provided here. The current studies were conducted on a home-built IMS-MS instrument. Solutions were electrosprayed by a TriVersa NanoMate autosampler (Advion, Ithaca, NY). The generated ions were trapped and accumulated in a Smith-geometry hourglass ion funnel.[77] Periodically, ion packets were introduced in short pulses (150 $\mu$s) into an ∼1.8 m long drift tube filled with ∼3.0 Torr of helium buffer gas at 300 K. Ions with different mobility were separated in the drift tube under the influence of a weak uniform electric field (∼10 V·cm$^{-1}$). Upon exiting the drift region, ions were extracted into an orthogonal reflectron time-of-flight mass spectrometer for flight time detection. As described previously, flight times in the mass analysis region are much


dx.doi.org/10.1021/ja505899g | J. Am. Chem. Soc. 2014, 136, 12702−12711

shorter than drift times, making it possible to collect the data in a nested fashion.[78]

**Determination of Collision Cross Sections.** Experimental drift times ($t_D$) can be converted into cross sections ($\Omega$) by using the following equation:[69]

$$\Omega = \frac{(18\pi)^{1/2}}{16}\frac{ze}{(k_bT)^{1/2}}\left[\frac{1}{m_I}+\frac{1}{m_B}\right]^{1/2}\frac{t_DE}{L}\frac{760}{P}\frac{T}{273.2}\frac{1}{N} \quad (1)$$

where $ze$ is the ion's charge, $k_b$ is Boltzmann's constant, and $T$ is the temperature of the buffer gas. Values $m_I$ and $m_B$ refer to the masses of the ion and the buffer gas (helium), respectively, and $N$ refers to the neutral number density of the buffer gas at STP. Parameters $E$, $L$, and $P$ correspond to the applied electric field, the length of the drift region, and the buffer gas pressure, respectively.

**Analysis of IMS-MS Data.** A method for IMS-MS data analysis was developed to investigate the transition routes of PPI converting into PPII in solution based on IMS-MS measurements. We started our analysis by finding the relative abundance of each of the eight different gas-phase conformers for the Pro13 $[M + 2H]^{2+}$ ions observed in the collision cross section distributions. This was achieved using the Peak Analyzer tool in OriginPro 9.0.0 software (OriginLab Corporation, Northampton, MA). According to the abundance profiles, several candidate transition routes were proposed. By applying the first-order reaction rate law to describe sequential and parallel reactions in a given candidate transition route, a differential equation was defined and solved for each conformer using Maple 17.01 software (Waterloo Maple Inc., Waterloo, Canada). The initial or boundary condition for each conformer was set as the abundance of that conformer obtained from the 1-propanol solution. The rate constants were the parameters of the resulting equations, and thus we determined the rate constants by fitting all of the abundance profile data to the equations using the Nonlinear Curve Fit tool in OriginPro 9.0.0. For each fitting, the maximum number of iterations was $5 \times 10^6$, and the tolerance was $1 \times 10^{-15}$. Among all of the candidate transition routes explored, the transition mechanism selected shows the best fitting for the IMS-MS data sets.

**Molecular Modeling and Cross Section Calculations.** Molecular dynamics (MD) simulations allow us to gain some insight about the solution-phase conformational changes of Pro13 along the PPI-to-PPII transition process. All the theoretical work was performed on Linux workstations using the program package of Insight II 2005 (Accelrys Inc., San Diego, CA). The initial geometries of Pro13 $[M + 2H]^{2+}$ ions with various distributions of *cis*/*trans* peptide bonds were generated by switching the bonds of an all-*cis* PPI helix ($\Phi$ = −83°, $\Psi$ = 158°, and $\omega$ = 0°) into the *trans* configurations of an all-*trans* PPII helix ($\Phi$ = −78°, $\Psi$ = 149°, and $\omega$ = 180°).[15] Based on prior IMS-MS structural analysis of the gas-phase PPI and PPII end conformations, the protons of each structure were assumed to be located on the N-terminus and the nitrogen atom of the sixth residue.[66] The preparation for simulation was performed in the Discover_3 module equipped with the extensible systematic force field (ESFF). MD simulations were carried out at 300 K for a minimum of 0.25 ns (up to 2.0 ns) using ESFF and a dielectric constant of 1.0. This procedure is analogous to our previous approach in which the relatively short time scales appear sufficient to obtain converged collective structural properties in *vacuo*.[66] Cross sections for the obtained lowest-energy conformations were then calculated by the trajectory method using MOBCAL (Indiana University, Bloomington, IN).[79] These calculated cross sections were compared to the experimental cross sections. The collision cross section of the structure chosen as the representative is within ±2.0% of the experimental value and has the smallest difference from the experimental value. The representative conformation should also be consistent with the transition mechanism determined from the IMS-MS analysis.

An issue that arises in MD studies is the large number of possible distributions of the *cis* and *trans* configurations along the backbone of the initial geometries. According to the candidate mechanisms proposed previously,[29,31,33] we prepared multiple conformations of polyprolines with various numbers and locations of *cis* and *trans* configurations. Due to the complexity of the polyproline conformation system, we did not sample all the possible structures of polyproline. However, the simulation work and the IMS-MS experiments presented here provide structural information for the transition process of polyproline converting from PPI into PPII. More details about the initial-geometry preparation are given below.

## RESULTS AND DISCUSSION

**Collision Cross Section Distribution of Pro13 $[M + 2H]^{2+}$ Ions at Different Transition Times.** The dominant ion formed by Pro13 upon electrospraying 1-propanol and water solutions is $[M + 2H]^{2+}$. Figure 2a and 2b show the collision cross section distribution of the detected Pro13 $[M + 2H]^{2+}$ ions as a function of time since dilution of a 1-propanol stock solution into an aqueous environment at 5 and 45 °C, respectively. The distributions recorded at different transition times for 15, 23, and 35 °C are shown in the Supporting Information. At each time point, the same solution is sampled; changes in the resulting gas-phase ion population therefore reflect changes in the source solution-phase population. Dashed lines in Figure 2 delimit the collision cross section distributions for assigned conformers (conformers A−H) used in subsequent data analysis; deviations from Gaussian distributions indicate that other conformers with very similar cross sections may be present within a given region. A summary of the collision cross sections of all of the observed $[M + 2H]^{2+}$ conformers is given in Table 1.

For comparison, time zero for the IMS-MS experiment is represented by the distribution generated from a 1-propanol solution of the same concentration (bottom of Figure 2a and 2b). Although some variations occur in the relative intensities of various conformers at different temperatures, conformer A dominates the distribution under all the conditions; conformer B and a small proportion of conformer C are also present. After dilution into the aqueous solution, a sequential loss of ions with larger collision cross sections is observed, with the concurrent appearance of more compact gas-phase conformers. Immediately upon dilution into water (time = 1 min) at 5 °C (Figure 2a), the distribution of Pro13 $[M + 2H]^{2+}$ ions shifts to give a broader distribution of conformer A, likely indicating multiple underlying structures, and a higher proportion of the unresolved peak representing the more compact conformers B and C. Over the first 29 min, the population of conformer A continues to decline, and conformers B and C become more abundant. By 150 min, the population of conformers B and C dominates, and conformer A has become vanishingly small. Conformer D starts to appear at this time. By 206 min, conformer A has completely disappeared. Conformers B and C continue to dominate the distribution, but conformer D has increased in abundance and the presence of more compact conformations (conformers E−G) is also first observed. Between 244 and 649 min, the fraction of conformers F and G increases dramatically, whereas a sharp decline in the relative abundance of conformers B and C is observed. At 649 min, the existence of conformer H is first observed, and the population of conformers D and E appears to decrease slightly. By 800 min, Pro13 $[M + 2H]^{2+}$ ions mainly adopt conformers F and G, and only a small amount of conformers D, E, and H are observed; no conformer B or C is seen. The collision cross section distribution of the ions then remains unchanged for an extended period of time (3000 min), suggesting that solution-phase equilibrium has been reached.

A comparison of Figure 2a to Figure 2b indicates that the same conformers are detected in the same relative order, but the transition occurs much more rapidly at higher temperatures.


dx.doi.org/10.1021/ja505899g | J. Am. Chem. Soc. 2014, 136, 12702−12711

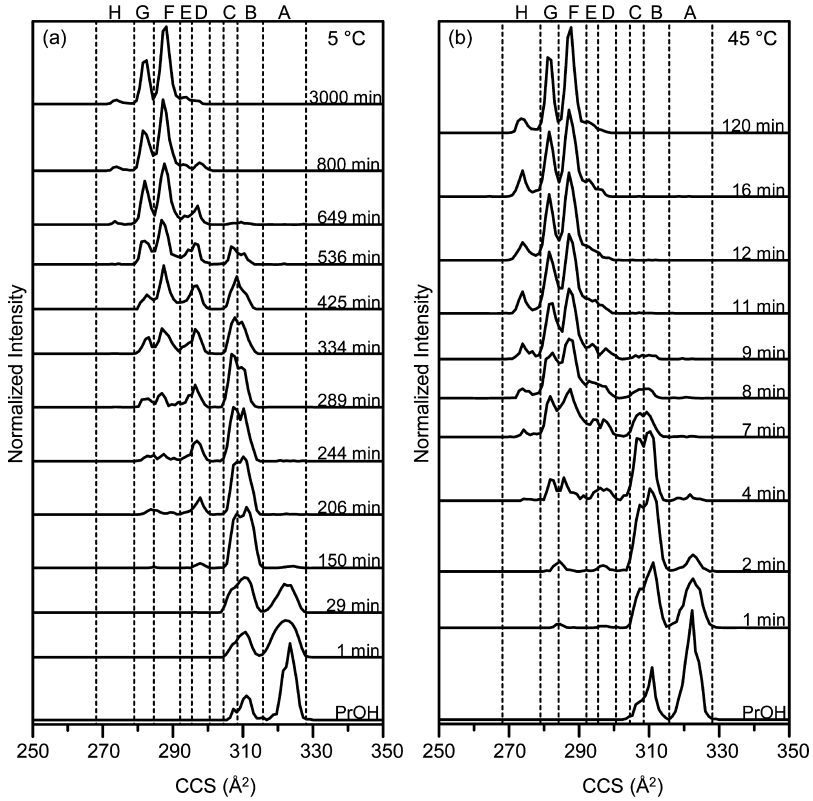


**Figure 2.** Collision cross section distributions for the $[M + 2H]^{2+}$ ions of Pro13 obtained at different transition times, showing the transition from PPI to PPII in 10:88:2 1-propanol/$H_2O$/HOAc (v/v/v) at 5 °C (a) and 45 °C (b). In order to illustrate the initial distributions for both transitions, the distributions for the ions formed by electrospraying 98:2 1-propanol/HOAc are also shown at the bottom of each panel. The transition times when the distributions were obtained are indicated in each trace, and dashed lines delineate the collision cross section region for each conformer type.

**Table 1. Summary of Collision Cross Sections of the Gas-Phase Conformers Observed for Pro13 $[M + 2H]^{2+}$ Ions Formed upon Electrospraying Aqueous and 1-Propanol Solutions**

| | | model geometries | | |
|---|---|---|---|---|
| assigned conformer | $\Omega_{expt}$ (Å$^2$) | initial geometry | *cis*/*trans* peptide bond distribution[a] | $\Omega_{calc}$ (Å$^2$) |
| A | 322 | PPI | CCCCCCCCCCCC | 324 |
| B | 312 | PPI′ | TTCCCCCCCCCC | 309 |
| C | 308 | PPI″ | TTTCCCCCCCCC | 306 |
| D | 297 | PPI–PPII | TTTCCTCCCCCC | 299 |
| E | 294 | PPII–PPI | TTTCCTTCCCCC | 293 |
| F | 288 | PPII | TTTTTTTTTTTT | 287 |
| G | 282 | PPII′ | TTTTTTTTCCCC | 282 |
| H | 273 | PPII″ | TTTTTTTTTTCT | 278 |

[a]The *cis*/*trans* peptide bond distribution along the backbone of the initial solution-phase geometry that generated the model gas-phase conformation is given here. "C" represents the *cis* form, and "T" corresponds to the *trans* configuration.

At 45 °C (Figure 2b), the population of conformers B and C has already exceeded that of conformer A after 1 min. By 2 min, most of the Pro13 $[M + 2H]^{2+}$ ions exist as conformers B and C, while the appearance of more compact conformations (conformers D–G) is seen. At 7 min, there is a significant increase in the relative abundance of conformers F and G, whereas conformer A completely disappears. Meanwhile, the populations of conformers D, E, and H appear to grow slowly, and the intensities of conformers B and C begin to decline. It is noted that conformers B and C remain present until 11 min, when conformers F, G, and H dominate the distribution for the Pro13 $[M + 2H]^{2+}$ ions. During this same time period, the relative abundance of conformers D and E gradually decreases. The completion of the transition process at 45 °C appears to occur at 16 min, and the obtained distribution is essentially identical with that measured at the longest time (120 min). For all of the experimental temperatures (5, 15, 23, 35, and 45 °C), we find similar transition processes, indicating that temperature is affecting the kinetics of the transition pathway rather than the mechanism itself.

We note that, at longer time periods, the parallel rise of two major and one minor compact conformation (conformers F, G, and H) is observed for all the transition processes studied; conformers D and E also remain as low-abundance peaks. As can be seen in the top portion of Figure 2a, this distribution is stable over a long period of time and is thus assumed to represent an equilibrium condition; analysis of samples 10 months after their preparation showed the same collision cross section distribution. The observation of multiple conformations at equilibrium is consistent with results from FRET[42] and molecular dynamics calculations[44−46] that postulate the presence of a stable heterogeneous population of PPII and PPII-like structures. As individual structures can be separately observed in this experiment, the proportion of each equilibrium conformer can be experimentally determined. NMR experiments have shown that ∼30% of Polyproline-20 molecules in aqueous solution contain an internal *cis* proline and a smaller proportion has a *cis* proline as the C-terminal residue.[42]


dx.doi.org/10.1021/ja505899g | J. Am. Chem. Soc. 2014, 136, 12702−12711

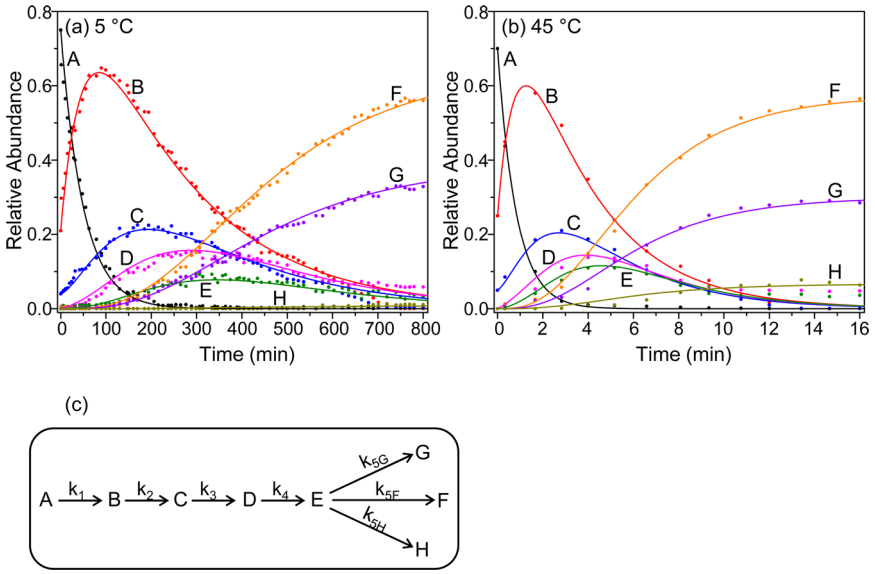


**Figure 3.** Relative abundance of different conformer types for the transition from PPI to PPII in 10:88:2 1-propanol/$H_2O$/HOAc (v/v/v) at 5 °C (a) and 45 °C (b) as a function of transition time, and the transition route used to fit the data points (c). In (a) and (b), the lines show the best fitting results, corresponding to the transition mechanism shown in (c). Various colors are used to represent different conformations: black is conformer A, red is conformer B, blue is conformer C, magenta is conformer D, olive is conformer E, orange is conformer F, violet is conformer G, and dark yellow is conformer H.

Although our experiment used a shorter polyproline peptide, we are able to observe a similar proportion of *cis*-containing polyproline in the equilibrium distribution; conformers G and H comprise ~33% of the total equilibrium population of Pro13 at room temperature (23 °C).

**Populations of Gas-Phase Conformers as a Function of Transition Time.** A more detailed analysis of the IMS-MS data is carried out by examining the relative abundance of the gas-phase conformers for the Pro13 $[M + 2H]^{2+}$ ions at different transition times. The relative abundance for all conformers (A–H), as determined by integrating the regions of our spectra associated with specific conformation types, are plotted in Figure 3a and 3b for the data obtained at 5 and 45 °C, respectively. Abundance profiles for the data recorded at 15, 23, and 35 °C are provided as Supporting Information. The mechanism shown in Figure 3c gives the best fit to the experimental data; as a comparison, in the Supporting Information, we show several fits of the data from mechanisms that do not fit the experimental findings. The solid lines in Figure 3a and 3b are the values of relative abundance calculated from a model of this mechanism, and they closely follow the experimental data. As part of the fitting, the rate constant for each step in the mechanism is calculated for each temperature (see Table S1). At 5 °C, the rate constants range from a high value of $(3.2 \pm 0.5) \times 10^{-4}$ $s^{-1}$ for $k_1$ to as low as $(5.6 \pm 2.0) \times 10^{-6}$ $s^{-1}$ for $k_{5H}$; at 45 °C, all of the rate constants are orders of magnitude greater, with values of $k_1 = (1.9 \pm 0.3) \times 10^{-2}$ $s^{-1}$ and $k_{5H} = (1.2 \pm 0.3) \times 10^{-3}$ $s^{-1}$.

To maintain stable electrospray conditions, 2% acetic acid was present in all solutions. Therefore, to ensure that our results were not due to the presence of the acid, the transition process was studied in the absence of acid at 23 °C (see Figures S7 and S8). The same transitions were observed, including the presence of two major conformers in the initial 1-propanol solution. Thus, these conformers and transitions are present with and without the small amount of acid in solution. The kinetics of the transition was also very similar, with rate constants within error of those found in the presence of acid for $k_1$ through $k_4$. However, the proportion of conformer G present at equilibrium was higher in the presence of acid, indicating that this conformer may be stabilized in acid.

Although temperature-induced isomerization of PPI to PPII has been observed in pure 1-propanol solutions, this process is found to be comparatively slow;[80] for amidated Polyproline-12, the overall rate constant for temperature-induced isomerization ranges from $1.5 \times 10^{-6}$ $s^{-1}$ at 5 °C to $1.4 \times 10^{-4}$ $s^{-1}$ at 45 °C. Compared with these values, our calculated rate constants for solvent-induced isomerization are large. As a result, solvent-induced isomerization should dominate the transition.

**Determination of Arrhenius Activation Parameters.** Arrhenius plots for the identified conformers in our IMS distribution are shown in Figure 4. The slope of the Arrhenius plot, $-E_a/R$, is similar for each transition step, indicating similar activation energies for each step in the mechanism (Table 2). The measured activation energies range from 71 ± 3 to 95 ± 11 kJ·$mol^{-1}$, values that are very similar to the previous reports of

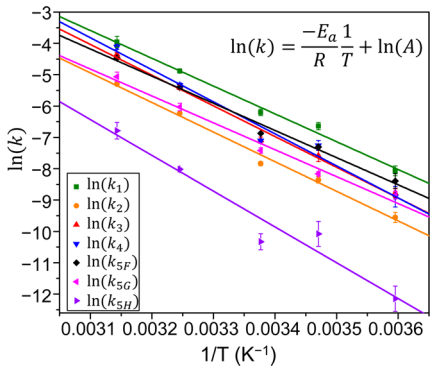


**Figure 4.** Arrhenius plot of the rate constants for the transition of Pro13 converting from PPI to PPII at five different temperatures (5, 15, 23, 35, and 45 °C). Error bars represent the standard deviation from triplicate analysis.


dx.doi.org/10.1021/ja505899g | J. Am. Chem. Soc. 2014, 136, 12702–12711

Table 2. Arrhenius Activation Energy, $E_a$, Preexponential Factor, $A$, and the Entropy of Activation, $\Delta S^{\ddagger}$, for Each Transition Step in the Proposed Mechanism

| Transition | Transition step[a] | $E_a$,[b] kJ·mol$^{-1}$ | $A$,[b] s$^{-1}$ | $\Delta S^{\ddagger}$,[c] J·mol$^{-1}$·K$^{-1}$ |
|---|---|---|---|---|
| 1 | PPI → PPI′ | 74 ± 4 | $10^{10.4\pm0.7}$ | −49 |
| 2 | PPI′ → PPI″ | 78 ± 2 | $10^{10.6\pm0.4}$ | −49 |
| 3 | PPI″ → PPI−PPII | 81 ± 2 | $10^{11.5\pm0.3}$ | −33 |
| 4 | PPI−PPII → PPII−PPI | 85 ± 7 | $10^{12.1\pm1.2}$ | −9 |
| 5F | PPII−PPI → PPII | 72 ± 3 | $10^{9.9\pm0.5}$ | −61 |
| 5G | PPII−PPI → PPII′ | 71 ± 3 | $10^{9.5\pm0.5}$ | −69 |
| 5H | PPII−PPI → PPII″ | 95 ± 11 | $10^{12.6\pm1.9}$ | 14 |

[a]The transition steps are associated with the solution-phase structures proposed in Figure 6. [b]Uncertainties correspond to one deviation about the mean for three independent measurements. [c]Values for the entropy of activation are calculated at 296.15 K using eq 2.

activation energies for a single *cis*−*trans* proline isomerization in acetyl-L-proline in aqueous solution (82.0 ± 0.4 kJ·mol$^{-1}$).[81] The formation of conformer H does have a higher activation barrier than the other transitions. Conformer H is also present in very low abundance at equilibrium, and as a result, the standard deviation of the calculated $E_a$ is also high. Despite the similarities of the barriers for each step, this cannot be a random process, because distinct conformers are found as a function of transition time. Our experimental results are also consistent with the calculated energy landscape of the previously reported zipper mechanism,[45] in which barriers are very similar in height and a global energy minimum is not reached.

In addition, as the intercept of the Arrhenius plot is $\ln(A)$, the value of the preexponential factor for each step in the transition mechanism is also determined. Table 2 shows that the calculated preexponential factor is similar for each step; the lowest value is $A_{5G}$ ($10^{9.5\pm0.5}$ s$^{-1}$), while $A_{5H}$ displays the highest value ($10^{12.6\pm1.9}$ s$^{-1}$). The calculated preexponential factors are also similar to values previously determined for the overall conversion of PPI to PPII by spectroscopic techniques (~$10^{12}$ s$^{-1}$).[20,82] Furthermore, using the relationship between the preexponential factor and the entropy of activation (eq 2) from transition state theory, the value for the entropy of activation ($\Delta S^{\ddagger}$) at 23 °C is also obtained for each step in the proposed mechanism (see Table 2).

$$A = \frac{ek_B T}{h} e^{\Delta S^{\ddagger}/R} \quad (2)$$

where $k_B$ is Boltzmann's constant, $T$ is the temperature at which the measurements were performed, $h$ is Planck's constant, $\Delta S^{\ddagger}$ is the entropy of activation, and $R$ is the gas constant. $\Delta S^{\ddagger}$ represents the difference between the entropy of each reactant or intermediate and its subsequent transition state; a negative value indicates that the system becomes somewhat more ordered at the transition state and suggests the presence of an entropic barrier. We note that except for $\Delta S^{\ddagger}_{5H}$, which has a positive value (14 J·mol$^{-1}$·K$^{-1}$), all of the calculated $\Delta S^{\ddagger}$ values are negative, indicating that there are both entropic and enthalpic barriers to folding along the pathway from PPI to PPII. Overall, these results are consistent with the idea that introduction of the PPI helix into an aqueous environment destabilizes the tight *cis*-configured helix; additional structure is obtained as the network of prolines flips into the *trans* configuration.

**Molecular Dynamics Simulations of Pro13 $[M + 2H]^{2+}$ Ions.** Due to the slow rate of *cis*−*trans* isomerization of proline, classical molecular dynamic (MD) simulations cannot be employed to follow the transition of polyproline in solution. To understand the conformational changes of Pro13 along the PPI-to-PPII transition pathway, we performed MD simulations of the Pro13 $[M + 2H]^{2+}$ ions in *vacuo* by building up candidate solution-phase structures that contain different combinations of *cis* and *trans* prolines. Here, we focus on comparing theoretical results with the IMS-MS data of the eight observed conformers. Figures 5 and 6 present the obtained representative gas-phase geometries and their corresponding initial solution-phase populations, respectively. A summary of the initial configurations and the calculated cross sections for the gas-phase conformations are given in Table 1. For comparison, the average and the standard deviation of the calculated cross sections for the 10 lowest-energy gas-phase conformations for every candidate solution-phase structure are also provided in the Supporting Information (Table S2).

We started our MD investigation with the all-*cis* PPI and all-*trans* PPII helices. According to the data obtained in our IMS-MS experiment, we suggest that conformers A and F correspond to the PPI and PPII helices, respectively, because their collision cross sections match the previously determined values for the PPI and PPII helices *in vacuo*.[66] Our simulation results appear to support this idea. The cross section calculated for the lowest-energy PPI-derived geometry (324 Å$^2$) is in very good agreement with the 322 Å$^2$ experimental values for conformer A; thus, this geometry was assigned as representative of conformer A. The lowest-energy geometry obtained from PPII was designated as conformer F because its calculated cross section is close to the experimental value ($\Omega_{calc}$ = 287 Å$^2$; $\Omega_{expt}$ = 288 Å$^2$). As is shown in Figure 5, the gas-phase conformer A contains the all-*cis* content of the PPI helix and is slightly stretched compared with the starting solution phase structure (Figure 6). This indicates that, in 1-propanol solution, the PPI helix is mainly stabilized by intramolecular interactions, which allows the helix to persist into the gas phase. On the other hand, the gas-phase conformer F is folded into a globular shape and is considerably more compact than an all-*trans* PPII helix. We note that the stabilization of the PPII helix in an aqueous environment is attributed to the hydrogen bonds established between the peptide and the solvent.[26] Upon removal of the solvent, the PPII helix collapses into a hairpin-like structure where hydrogen bonds could be formed between charge sites and carbonyl groups on the backbone. These findings are consistent with earlier theoretical work on anhydrous PPI and PPII helices.[66]

In addition to conformers A and F, six different conformer types (conformers B, C, D, E, G, and H) were found in the IMS-MS experiments, reflecting the existence of other Pro13 subpopulations in solution. Our kinetic model is in agreement with prior results that indicate that the transition likely follows a mechanism in which the isomerization of peptide bonds occurs in a sequential fashion.[31,32] Additionally, prior simulation studies imply four possible mechanisms for the PPI-to-PPII

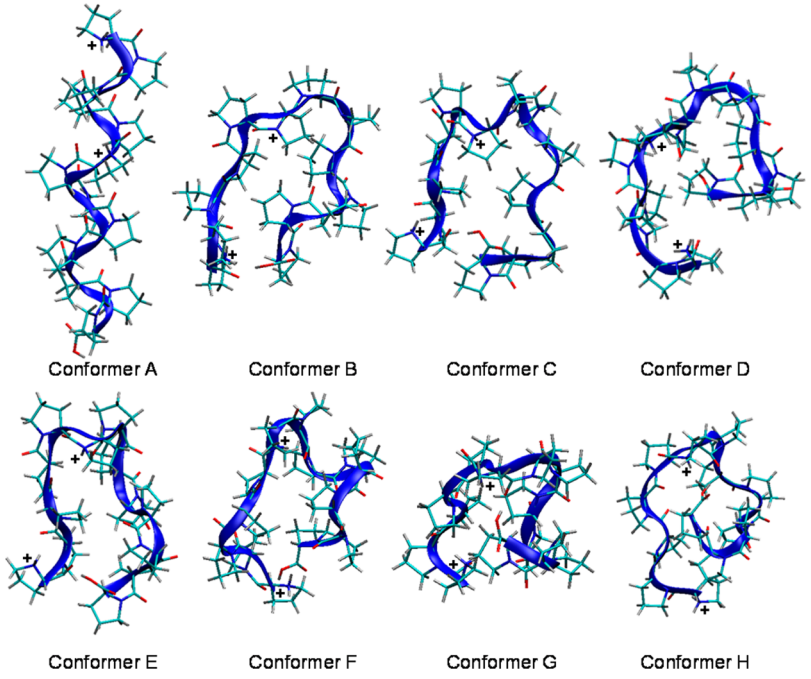


**Figure 5.** Representative Pro13 $[M + 2H]^{2+}$ conformers obtained via 300 K gas-phase molecular dynamic simulations of the initial geometries shown in Figure 6. The charge sites were assigned on the N-terminus and the nitrogen atom of the sixth residue. The initial structures for conformer A and F were PPI and PPII helices, respectively. Conformer B was obtained from PPI′, conformer C was obtained from PPI′′, and conformer D was obtained from PPI−PPII. PPII−PPI, PPII′, and PPII′′ were the starting geometries for conformer E, G, and H, respectively.

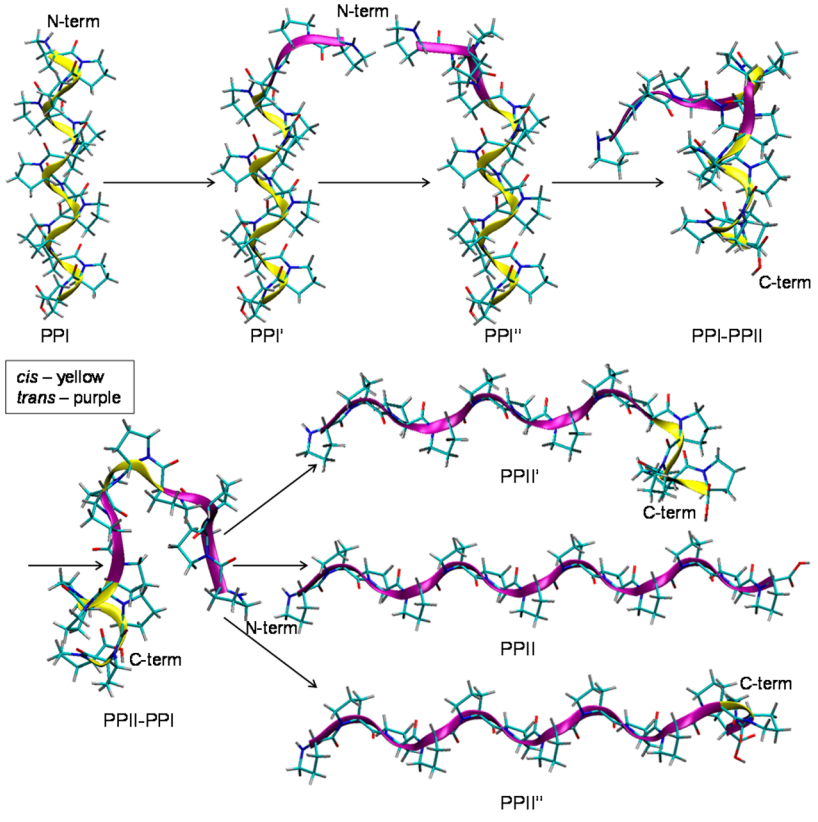


**Figure 6.** Proposed mechanism for Pro13 converting from PPI to PPII. The *cis* residues are shown as yellow ribbons, while the *trans* residues are shown as purple ribbons. See text for details.

transition of polyproline: starting from the N-terminus, starting from the C-terminus, starting from both termini, and starting from the center of the peptide backbone.[31,45,46] Based on these mechanisms, we carried out the initial geometry preparation for the observed Pro13 subpopulations by sequentially flipping the *cis* prolines of a PPI helix into the *trans* prolines of an all-*trans*


dx.doi.org/10.1021/ja505899g | J. Am. Chem. Soc. 2014, 136, 12702−12711

PPII helix. There are two different pathways for the mechanisms starting from both termini: either the N-terminus or the C-terminus could flip first. Similarly, since the number of peptide bonds is even for Pro13, there are two different pathways starting from the center of the peptide chain; the first flip could occur closer to the N-terminus or closer to the C-terminus. Consequently, we created 52 various starting structures as candidate Pro13 subpopulations in solution.

After performing MD simulations for the prepared structures *in vacuo*, we obtained a number of lowest-energy conformations that display cross sections within 2% of the experimentally determined cross sections. According to our kinetic model, these conformers, however, should also follow a sequential transition mechanism. More specifically, we assume that *trans* to *cis* isomerization is highly disfavored in aqueous solution. As the mechanism proceeds, the peptide bonds that have already isomerized may not revert to *cis* and thus further isomerizations can only occur on remaining *cis* peptide bonds. The starting structures (Figure 6) of the *in vacuo* conformations B and C (Figure 5) are considered as possible intermediates along a PPI-to-PPII transition pathway involving sequential *cis* to *trans* isomerism starting at the N-terminus. Gas-phase structures corresponding to the first two steps of other potential pathways (starting at the C-terminus, starting at both termini, and starting at the middle of the peptide) were not consistent with our experimental collision cross sections. The first model structure is for conformer B (Figure 5); it has a calculated cross section of 309 Å$^2$, showing a good agreement with the value measured in IMS-MS experiments ($\Omega_{exp}$ = 312 Å$^2$). We named the initial configuration of conformer B as PPI′ because it was generated by flipping the first two peptide bonds at the N-terminus of a PPI helix from *cis* to *trans*. The second conformation is for conformer C; its calculated cross section is also consistent with the experimental value ($\Omega_{calc}$ = 306 Å$^2$; $\Omega_{exp}$ = 308 Å$^2$). The initial solution phase geometry of conformer C was assigned as PPI′′, as the first three peptide bonds at the N-terminus are in *trans* form while the others retain the *cis* bonds of a PPI helix. A comparison between the obtained gas-phase structures (Figure 5) and their corresponding solution-phase configurations (Figure 6) shows that conformers B and C appear to adopt relatively compact geometries as the solvent is removed. A mixture of *cis* and *trans* residues in the solution-phase polymer contributes to these compact gas-phase conformations, but there was no obvious correlation between the position of solution-phase isomerization and the resulting gas-phase structure. Further analysis reveals that the folded gas-phase geometries of conformers B and C allow hydrogen-bonding interactions to be established between the protonation sites and the backbone carbonyls.

Experimental collision cross sections of subsequent conformers are not in agreement with geometries generated by MD simulations corresponding to further sequential flipping of peptide bonds from the N-terminus. The PPI-to-PPII transition of Pro13 in solution is therefore more complex than expected. In our proposed transition scheme (Figure 3c), conformer C serves as the precursor for the indeterminate conformers. The sequential nature of our mechanism indicates that the isomerization(s) to form conformer D must occur in the remaining *cis* peptide bonds in the initial solution-phase structure of conformer C, PPI′′. Therefore, potential solution subpopulations of Pro13 were further explored by randomly varying the remaining *cis* proline residues in PPI′′ into *trans* proline residues. The helix created by flipping the sixth peptide bond of PPI′′ into *trans* form yields a lowest-energy geometry that is in closest agreement with conformer D ($\Omega_{calc}$ = 299 Å$^2$; $\Omega_{exp}$ = 297 Å$^2$). Consequently, the obtained gas-phase configuration is used to represent conformer D, and its starting structure is named as PPI–PPII. A viable representation discovered for conformer E ($\Omega_{calc}$ = 293 Å$^2$) also matches the experimental value ($\Omega_{exp}$ = 294 Å$^2$) and was derived from the structure where the seventh peptide bond of PPI–PPII is switched into *trans* form. We consider this solution subpopulation as PPII–PPI. In our proposed mechanism, the isomerization of PPII–PPI can form three conformers in parallel, one of which is the all-*trans* PPII corresponding to conformer F. A viable representation for conformer G ($\Omega_{calc}$ = $\Omega_{exp}$ = 282 Å$^2$) was derived from an initial solution-phase structure comprising eight *trans* peptide bonds at the N-terminus and only four *cis* peptide bonds at the C-terminus. This structure was labeled as PPII′; mechanistically, it is formed by flipping the fourth, fifth, and eighth peptide bonds of PPII–PPI to *trans* form. Additionally, when the 11th peptide bond of an all-*trans* PPII helix is in the *cis* configuration, it leads to a lowest-energy conformation with a cross section of 278 Å$^2$ that is slightly higher than that of conformer H ($\Omega_{exp}$ = 273 Å$^2$). This allowed us to provide a candidate configuration for conformer H and assign its corresponding solution structure as PPII′′. Compared with the solution states, the gas-phase geometries adopted by conformers D, E, G, and H are more compact, and the position of the bend appears to occur at the charge site. We also note that, except for conformer A that maintains a PPI-like configuration, all the other dehydrated conformations favor globular and hairpin-like geometries to increase van der Waals stabilization and accommodate hydrogen bonding between charge sites and carbonyl groups on the peptide backbone.

**The PPI-to-PPII Transition Mechanism of Pro13 in Solution.** By combining the solution populations obtained via simulation with the IMS-MS analysis results, we present one possible transition mechanism for Pro13 converting from PPI into PPII in aqueous solution. Figure 6 shows the proposed mechanism with detailed conformational context, and activation energy barriers for each step are shown in Table 2. The transition of Pro13 starts from an all-*cis* PPI helix. The first two peptide bonds at the N-terminus of PPI switch into the *trans* form to generate the first intermediate PPI′; the energy barrier of this step is 74 ± 4 kJ·mol$^{-1}$. Then the third peptide bond of PPI′ flips into the *trans* configuration, overcoming an energy barrier of 78 ± 2 kJ·mol$^{-1}$ and leading to another subpopulation, PPI′′. It is interesting that the second transition step, in which only one proline residue isomerizes, has a similar energy barrier value to the first step. This finding reflects that the N-terminal region of the PPI helix is considerably flexible, which may contribute to the presence of multiple conformer types observed in 1-propanol solution.

The following transition step creates the third intermediate structure, PPI–PPII; in this step, the sixth peptide bond of PPI′′ converts into the *trans* configuration and overcomes an energy barrier of 81 ± 2 kJ·mol$^{-1}$. Next, the seventh peptide bond of PPI–PPII changes into the *trans* configuration; this has a similar energy barrier value to the previous step (85 ± 7 kJ·mol$^{-1}$). Both PPI–PPII and PPII–PPI display significantly different structures compared with PPI due to the transition from *cis* to *trans* occurring at the center of the peptide backbone. At the end of the transition process, there are three parallel converting steps. With an energy barrier of 72 ± 3 kJ·mol$^{-1}$, all the remaining *cis* residues in PPII–PPI can convert into the *trans* configuration, generating

the all-*trans* PPII helix. Another possible transition step is the formation of PPII′, in which the four peptide bonds at the C-terminus remain in the *cis* form. The energy barrier of this step ($71 \pm 3$ kJ·mol$^{-1}$) is very similar to that of the step where the PPII helix is formed ($72 \pm 3$ kJ·mol$^{-1}$), indicating that the C-terminal region of the polypeptide is also quite flexible. However, the transition step that creates PPII′′ displays a significantly higher energy barrier ($95 \pm 11$ kJ·mol$^{-1}$), and the generated PPII′′ only includes one internal peptide bond (the 11th peptide bond) in the *cis* configuration.

Our results indicate that the mechanism of Pro13 conversion from PPI into PPII likely starts from the N-terminus, followed by isomerization at the center of the peptide backbone. This is in contrast to recent theoretical work on smaller polyproline peptides that shows that the transition process could move inward from both termini, starting with the N-terminus.[31] For Pro13, our data do not support this mechanism because the gas-phase conformers created from the solution populations that correspond to this mechanism have calculated cross sections that are not in agreement with experimental values.

## CONCLUSIONS

IMS-MS and molecule modeling have been used to examine the structural transition of a 13-residue polyproline peptide (Pro13). Evidence is found for distinct intermediates along the transition pathway for the conversion from PPI to PPII. Collision cross sections of the gas-phase structures of these intermediates are consistent with a transition mechanism for Pro13 isomerization from PPI into PPII that starts from the N-terminus. This result is consistent with previous enzymatic studies[33] but contradicts the results of previous NMR studies.[29] The transition process of Pro13 is also complicated. Since the PPI helix has 3.3 residues per turn, our proposed mechanism suggests that, once the first turn of PPI involving the first three peptide bonds has flipped into the *trans* configuration, the next step of the transition could take place in the middle of the peptide backbone. It is notable that significant changes of configuration occur during the formation and disappearance of the intermediates PPI−PPII and PPII−PPI. This finding is in good agreement with polyproline transition experiments performed using circular dichroism and other optical spectroscopies, in which a spectroscopically distinct intermediate was detected.[23] Our proposed transition mechanism fits with our experimental kinetic data and is consistent with probable transitions in the solution state. Although we cannot entirely rule out other more random solution-state transitions that may give rise to gas-phase ion conformations with similar collision cross sections, we are able to demonstrate the presence of multiple discrete intermediates along the transition pathway. The energy landscape in the transition appears to be very similar for each step; only the step in which the PPII′′ helix is formed shows a relatively higher energy barrier ($95 \pm 11$ kJ·mol$^{-1}$). This barrier is consistent with the relatively low-abundance of conformer H in the IMS-MS data. Additionally, we find that, at the end of the transition, two stable subpopulations coexist with the all-*trans* PPII helix, a result that is consistent with previous FRET and simulation work that suggested the presence of stable subpopulations for the PPII helix.[32,40−42,44−46]

## ASSOCIATED CONTENT

### Supporting Information

Two fits of the data from the mechanisms that do not fit the experimental findings; the distributions recorded at different transition times for 15, 23, and 35 °C; the abundance profiles for 15, 23, and 35 °C; the distributions recorded at different transition times and the abundance profiles for 23 °C in the absence of acid; the calculated rate constant for each step in the proposed mechanism for the five temperatures explored; and a summary of all the candidate solution-phase structures prepared in the simulation and the calculated cross sections for their gas-phase conformations. This material is available free of charge via the Internet at http://pubs.acs.org.

## AUTHOR INFORMATION


### Corresponding Author

clemmer@indiana.edu

### Present Address

[‖]Chemistry Department, Moravian College, Bethlehem, Pennsylvania 18018, United States.


### Notes

The authors declare no competing financial interest.

## ACKNOWLEDGMENTS

We gratefully thank David Smiley and the DiMarchi Laboratory at Indiana University for assistance with the peptide synthesis used in this work. This research was supported in part by a grant from the Indiana University METACyt initiative, funded by the Lilly Endowment.

## REFERENCES


(1) *Poly-α-amino Acids*; Fasman, G. D., Ed.; M. Dekker: New York, 1967.
(2) Schimmel, P. R.; Flory, P. J. *Proc. Natl. Acad. Sci. U.S.A.* **1967**, *58*, 52−59.
(3) Jabs, A.; Weiss, M. S.; Hilgenfeld, R. *J. Mol. Biol.* **1999**, *286*, 291−304.
(4) Fischer, G. *Chem. Soc. Rev.* **2000**, *29*, 119−127.
(5) Wedemeyer, W. J.; Welker, E.; Scheraga, H. A. *Biochemistry* **2002**, *41*, 14637−14644.
(6) Andreotti, A. H. *Biochemistry* **2003**, *42*, 9515−9524.
(7) Dugave, C.; Demange, L. *Chem. Rev.* **2003**, *103*, 2475−2532.
(8) Lummis, S. C. R.; Beene, D. L.; Lee, L. W.; Lester, H. A.; Broadhurst, R. W.; Dougherty, D. A. *Nature* **2005**, *438*, 248−252.
(9) Lu, K. P.; Finn, G.; Lee, T. H.; Nicholson, L. K. *Nat. Chem. Biol.* **2007**, *3*, 619−629.
(10) Sarkar, P.; Reichman, C.; Saleh, T.; Birge, R. B.; Kalodimos, C. G. *Mol. Cell* **2007**, *25*, 413−426.
(11) Schmid, F. Prolyl Isomerization in Protein Folding. In *Protein Folding Handbook*; Buchner, J., Kiefhabe, T., Eds.; Wiley-VCH Verlag GmbH: Weinheim, Germany, 2008; pp 916−945.
(12) Baldwin, R. L. *Annu. Rev. Biophys.* **2008**, *37*, 1−21.
(13) Craveur, P.; Joseph, A. P.; Poulain, P.; de Brevern, A. G.; Rebehmed, J. *Amino Acids* **2013**, *45*, 279−289.
(14) Theillet, F. X.; Kalmar, L.; Tompa, P.; Han, K. H.; Selenko, P.; Dunker, A. K.; Daughdrill, G. W.; Uversky, V. N. *Intrinsically Disordered Proteins* **2013**, *1*, e243601−e2436013.
(15) IUPAC-IUB Commission on Biochemical Nomenclature. *Biochemistry* **1970**, *9*, 3471−3479.
(16) Kurtz, Z.; Berger, A.; Katchalski, E. *Nature* **1956**, *178*, 1066−1067.
(17) Harrington, W. F.; Sela, M. *Biochim. Biophys. Acta* **1958**, *27*, 24−41.
(18) Steinberg, I. Z.; Harrington, W. F.; Berger, A.; Sela, M.; Roberts, D. E. *J. Am. Chem. Soc.* **1960**, *82*, 5263−5279.
(19) Gornick, F.; Mandelkern, L.; Dorio, A. F.; Roberts, D. E. *J. Am. Chem. Soc.* **1964**, *86*, 2549−2555.
(20) Engel, J. *Biopolymers* **1966**, *4*, 945−948.
(21) Conti, E.; Piatelli, M.; Viglino, P. *Biopolymers* **1969**, *7*, 411−415.

(22) Ganser, V.; Engel, J.; Winklmair, D.; Krause, G. *Biopolymers* **1970**, *9*, 329−352.
(23) Dukor, R. A.; Keiderling, T. A. *Biospectroscopy* **1996**, *2*, 83−100.
(24) Kakinoki, S.; Hirano, Y.; Oka, M. *Polym. Bull.* **2005**, *53*, 109−115.
(25) Traub, W.; Shmueli, U. *Nature* **1963**, *198*, 1165−1166.
(26) Swenson, C. A.; Formanek, R. *J. Phys. Chem.* **1967**, *71*, 4073−4077.
(27) Forsythe, K. H.; Hopfinger, A. J. *Macromolecules* **1973**, *6*, 423−437.
(28) Rifkind, J. M.; Applequist, J. *J. Am. Chem. Soc.* **1968**, *90*, 3650−3654.
(29) Torchia, D. A.; Bovey, F. A. *Macromolecules* **1971**, *4*, 246−251.
(30) Profant, V.; Baumruk, V.; Li, X.; Šafařík, M.; Bouř, P. *J. Phys. Chem. B* **2011**, *115*, 15079−15089.
(31) Moradi, M.; Babin, V.; Roland, C.; Sagui, C. *J. Chem. Phys.* **2010**, *133*, 125104−125122.
(32) Kang, Y. K.; Jhon, J. S.; Park, H. S. *J. Phys. Chem. B* **2006**, *110*, 17645−17655.
(33) Lin, L. N.; Brandts, J. F. *Biochemistry* **1980**, *19*, 3055−3059.
(34) Rath, A.; Davidson, A. R.; Deber, C. M. *Biopolymers (Peptide Science)* **2005**, *80*, 179−185.
(35) Shi, Z.; Chen, K.; Liu, Z.; Kallenbach, N. R. *Chem. Rev.* **2006**, *106*, 1877−1897.
(36) Shoulders, M. D.; Raines, R. T. *Annu. Rev. Biochem.* **2009**, *78*, 929−958.
(37) Schweitzer-Stenner, R. *Mol. BioSyst.* **2012**, *8*, 122−133.
(38) Adzhubei, A. A.; Sternberg, M. J. E.; Makarov, A. A. *J. Mol. Biol.* **2013**, *425*, 2100−2132.
(39) Stryer, L.; Haugland, R. P. *Proc. Natl. Acad. Sci. U.S.A.* **1967**, *58*, 719−726.
(40) Schuler, B.; Lipman, E. A.; Steinbach, P. J.; Kumke, M.; Eaton, W. A. *Proc. Natl. Acad. Sci. U.S.A.* **2005**, *102*, 2754−2759.
(41) Watkins, L. P.; Chang, H.; Yang, H. *J. Phys. Chem. A* **2006**, *110*, 5191−5203.
(42) Best, R. B.; Merchant, K. A.; Gopich, I. V.; Schuler, B.; Bax, A.; Eaton, W. A. *Proc. Natl. Acad. Sci. U.S.A.* **2007**, *104*, 18964−18969.
(43) Doose, S.; Neuweiler, H.; Barsch, H.; Sauer, M. *Proc. Natl. Acad. Sci. U.S.A.* **2007**, *104*, 17400−17405.
(44) Radhakrishnan, A.; Vitalis, A.; Mao, A. H.; Steffen, A. T.; Pappu, R. V. *J. Phys. Chem. B* **2012**, *116*, 6862−6871.
(45) Moradi, M.; Babin, V.; Roland, C.; Darden, T. A.; Sagui, C. *Proc. Natl. Acad. Sci. U.S.A.* **2009**, *106*, 20746−20751.
(46) Moradi, M.; Lee, J. G.; Babin, V.; Roland, C.; Sagui, C. *Int. J. Quantum Chem.* **2010**, 2865−2879.
(47) Hoaglund-Hyzer, C. S.; Counterman, A. E.; Clemmer, D. E. *Chem. Rev.* **1999**, *99*, 3037−3079.
(48) Bohrer, B. C.; Merenbloom, S. I.; Koeniger, S. L.; Hilderbrand, A. E.; Clemmer, D. E. *Annu. Rev. Anal. Chem.* **2008**, *1*, 293−327.
(49) Wyttenbach, T.; Pierson, N. A.; Clemmer, D. E.; Bowers, M. T. *Annu. Rev. Phys. Chem.* **2014**, *65*, 175−196.
(50) Lanucara, F.; Holman, S. W.; Gray, C. J.; Eyers, C. E. *Nat. Chem.* **2014**, *6*, 208−215.
(51) Baumketner, A.; Bernstein, S. L.; Wyttenbach, T.; Bitan, G.; Teplow, D. B.; Bowers, M. T.; Shea, J.-E. *Protein Sci.* **2006**, *15*, 420−428.
(52) Ruotolo, B. T.; Robinson, C. V. *Curr. Opin. Chem. Biol.* **2006**, *10*, 402−408.
(53) Wyttenbach, T.; Bowers, M. T. *J. Phys. Chem. B* **2011**, *115*, 12266−12275.
(54) Pierson, N. A.; Chen, L.; Valentine, S. J.; Russell, D. H.; Clemmer, D. E. *J. Am. Chem. Soc.* **2011**, *133*, 13810−13813.
(55) Shi, H.; Pierson, N. A.; Valentine, S. J.; Clemmer, D. E. *J. Phys. Chem. B* **2012**, *116*, 3344−3352.
(56) Hall, Z.; Politis, A.; Bush, M. F.; Smith, L. J.; Robinson, C. V. *J. Am. Chem. Soc.* **2012**, *134*, 3429−3438.
(57) Silveira, J. A.; Fort, K. L.; Pierson, N. A.; Clemmer, D. E.; Russell, D. H. *J. Am. Chem. Soc.* **2013**, *135*, 19147−19153.
(58) Johnson, R. S.; Martin, S. A.; Biemann, K. *Int. J. Mass Spectrom. Ion Processes* **1988**, *86*, 137−154.
(59) Loo, J. A.; Edmonds, C. G.; Smith, R. D. *Science* **1990**, *248*, 201−204.
(60) Covey, T.; Douglas, D. J. *J. Am. Soc. Mass Spectrom.* **1993**, *4*, 616−623.
(61) Suckau, D.; Shi, Y.; Beu, S. C.; Senko, M. W.; Quinn, J. P.; Wampler, F. M.; McLafferty, F. W. *Proc. Natl. Acad. Sci. U.S.A.* **1993**, *90*, 790−793.
(62) Syka, J. E. P.; Coon, J. J.; Schroeder, M. J.; Shabanowitz, J.; Hunt, D. F. *Proc. Natl. Acad. Sci. U.S.A.* **2004**, *101*, 9528−9533.
(63) Pan, Y.; Brown, L.; Konermann, L. *Int. J. Mass Spectrom.* **2011**, *302*, 3−11.
(64) Chen, L.; Gao, Y. Q.; Russell, D. H. *J. Phys. Chem. A* **2012**, *116*, 689−696.
(65) Bleiholder, C.; Do, T. D.; Wu, C.; Economou, N. J.; Bernstein, S. S.; Buratto, S. K.; Shea, J.-E.; Bowers, M. T. *J. Am. Chem. Soc.* **2013**, *135*, 16926−16937.
(66) Counterman, A. E.; Clemmer, D. E. *J. Phys. Chem. B* **2004**, *108*, 4885−4898.
(67) Chandrudu, S.; Simerska, P.; Toth, I. *Molecules* **2013**, *18*, 4373−4388.
(68) Ye, Y.; Li, H.; Jiang, X. *Biopolymers (Peptide Science)* **2005**, *80*, 172−178.
(69) Mason, E. A.; McDaniel, E. W. *Transport Properties of Ions in Gases*; Wiley: New York, 1988.
(70) Revercomb, H. E.; Mason, E. A. *Anal. Chem.* **1975**, *47*, 970−983.
(71) Shvartsburg, A. A.; Jarrold, M. F. *Chem. Phys. Lett.* **1996**, *261*, 86−91.
(72) Mesleh, M. F.; Hunter, J. M.; Shvartsburg, A. A.; Schatz, G. C.; Jarrold, M. F. *J. Phys. Chem.* **1996**, *100*, 16082−16086.
(73) Wyttenbach, T.; von Helden, G.; Batka, J. J.; Carlat, D.; Bowers, M. T. *J. Am. Soc. Mass Spectrom.* **1997**, *8*, 275−282.
(74) McLean, J. A.; Ruotolo, B. T.; Gillig, K. J.; Russell, D. H. *Int. J. Mass Spectrom.* **2005**, *240*, 301−315.
(75) Tang, K.; Shvartsburg, A. A.; Lee, H. N.; Prior, D. C.; Buschbach, M. A.; Li, F. M.; Tolmachev, A. V.; Anderson, G. A.; Smith, R. D. *Anal. Chem.* **2005**, *77*, 3330−3339.
(76) Kanu, A. B.; Dwivedi, P.; Tam, M.; Matz, L.; Hill, H. H. *J. Mass Spectrom.* **2008**, *43*, 1−22.
(77) Shaffer, S. A.; Tang, K. Q.; Anderson, G. A.; Prior, D. C.; Udseth, H. R.; Smith, R. D. *Rapid Commun. Mass Spectrom.* **1997**, *11*, 1813−1817.
(78) Hoaglund, C. S.; Valentine, S. J.; Sporleder, C. R.; Reilly, J. P.; Clemmer, D. E. *Anal. Chem.* **1998**, *70*, 2236−2242.
(79) Mesleh, M. F.; Hunter, J. M.; Shvartsburg, A. A.; Schatz, G. C.; Jarrold, M. F. *J. Phys. Chem.* **1996**, *100*, 16082−16086.
(80) Kuemin, M.; Engel, J.; Wennemersa, H. *J. Pept. Sci.* **2010**, *16*, 596−600.
(81) Cheng, H. N.; Bovey, F. A. *Biopolymers* **1977**, *16*, 1465−1472.
(82) Downie, A. R.; Randall, A. A. *Trans. Faraday Soc.* **1959**, *55*, 2132−2140.